DOI: 10.1534/genetics.107.085977

A Suppressor Screen in Chlamydomonas Identifies Novel Components of the Retinoblastoma Tumor Suppressor Pathway

Su-Chiung Fang and James G. Umen[1]

Plant Biology Laboratory, The Salk Institute, La Jolla, California 92037

Manuscript received December 14, 2007
Accepted for publication December 19, 2007

ABSTRACT

The retinoblastoma (RB) protein is a eukaryotic tumor suppressor and negative cell-cycle regulator. *Chlamydomonas reinhardtii* cells that lack the RB homolog MAT3 show loss of size checkpoint control and deregulated cell-cycle progression leading to the production of tiny cells. We carried out an insertional mutagenesis screen to isolate bypass *s*uppressors of ***mat3*** (*smt* mutants) that reverted the *mat3* cell-size defect. Previously we reported that the loci encoding Chlamydomonas homologs of E2F and DP were frequently disrupted in this screen, indicating that the architecture of the canonical RB pathway is conserved in Chlamydomonas with MAT3/RB acting as a negative regulator upstream of E2F/DP. Here, we describe four novel *smt* mutants that moderately suppressed the cell-size checkpoint and cell-cycle phenotypes of *mat3*. As single mutants, three of the *smt* strains displayed no obvious phenotypes, and one had a slightly small phenotype. Strikingly, several *smt* double-mutant combinations synergized to cause enhanced suppression of *mat3* and even to cause a large-cell phenotype that is comparable to that caused by loss of DP1. Molecular characterization of one *smt* mutant revealed that suppression is due to a defect in a gene encoding a putative small ubiquitin-like modifier (SUMO) peptidase. Our results reveal a complex genetic network that lies downstream of MAT3/RB and implicate protein sumoylation as an important step for cell-cycle progression in cells that are missing MAT3/RB.

THE retinoblastoma (RB) protein is a tumor suppressor and negative cell-cycle regulator that is conserved in animals, plants, green algae, and other eukaryotic lineages, but has been lost from yeasts and other fungi. In the past two decades intensive efforts have been made to understand how RB regulates cell-cycle progression, cell proliferation, differentiation, and development.

The canonical RB pathway involves the cell-cycle-regulated interaction of RB or its homologs (also called pocket proteins) with a heterodimeric transcription factor composed of E2F and DP subunits. The RB-associated E2F/DP protein complex represses transcription of cell-cycle genes, and this repression is released by removal of RB via phosphorylation. Subsequently, E2F/DP-dependent transcription of cell-cycle genes allows S-phase entry and cell-cycle progression (Weinberg 1995; Harbour and Dean 2000; Knudsen and Knudsen 2006).

Genetic screens in the fruit fly *Drosophila melanogaster* and in the roundworm *Caenorhabditis elegans* have led to new insights into the RB pathway, including the identification of functions that are cell-cycle independent (Lu and Horvitz 1998; Staehling-Hampton *et al.* 1999; Ceol and Horvitz 2001; Fay *et al.* 2002; Bender *et al.* 2004, 2007; Cui *et al.* 2004, 2006; Andersen *et al.* 2006; Korenjak and Brehm 2006; Ceron *et al.* 2007; Reddien *et al.* 2007), some of which may be mediated by a recently identified pocket protein complex that is conserved in animals and acts as a transcriptional regulator (Korenjak *et al.* 2004; Lewis *et al.* 2004; Litovchick *et al.* 2007). These and other studies have shed light on the complicated transcriptional network that is governed by pocket proteins and that regulates various classes of target genes including cell-cycle genes, DNA damage-response genes, differentiation-associated genes, and others (Lavia and Jansen-Durr 1999; Stevaux and Dyson 2002; Cam and Dynlacht 2003; Ramirez-Parra *et al.* 2003; Blais and Dynlacht 2004; Bracken *et al.* 2004; Chaussepied and Ginsberg 2005; Dimova and Dyson 2005; Vandepoele *et al.* 2005). In higher plants the RB–E2F pathway is also critical for cell-cycle progression and development, but much less is known about plant pocket protein complexes and their regulation (Ebel *et al.* 2004; Park *et al.* 2005; Wildwater *et al.* 2005; Wyrzykowska *et al.* 2006; Jordan *et al.* 2007). Thus, despite recent advances many questions about the RB pathway remain open, including the identification of key targets that are important for cell-cycle progression and tumorigenesis (Knudsen and Knudsen 2006).

The unicellular green alga *Chlamydomonas reinhardtii* is a simple, genetically tractable model organism that

[1]*Corresponding author:* Plant Biology Laboratory, The Salk Institute for Biological Studies, 10010 N. Torrey Pines Rd., La Jolla, CA 92037. E-mail: umen@salk.edu

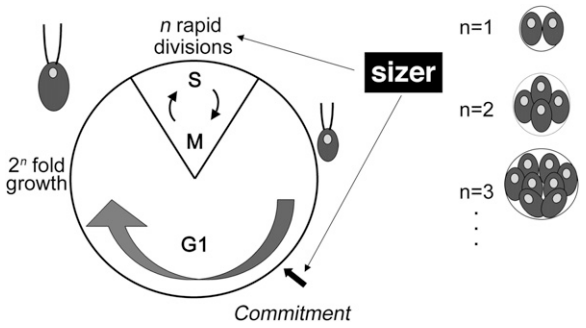

Figure 1.—Chlamydomonas multiple-fission cell cycle. See the Introduction for details.

has the key components of the RB pathway (Bisova *et al.* 2005), including a single RB homolog encoded by the *MAT3* locus (Umen and Goodenough 2001). Our previous studies have demonstrated that the architecture of the canonical RB pathway is conserved in Chlamydomonas with E2F1-DP1 acting as positive regulators downstream of RB/MAT3 (Fang *et al.* 2006). Moreover, although they have severe cell-cycle phenotypes, null mutations in *MAT3* and *DP1* are viable, thus facilitating genetic analyses.

Chlamydomonas proliferates using a multiple-fission cell cycle (Figure 1) that partially uncouples growth and division. The multiple-fission cell cycle is characterized by a long G_1 period during which cells can grow many-fold in size. At the end of G_1, mother cells undergo one or more rapidly alternating rounds of S phase and mitosis (S/M) to produce 2^n daughters of uniform size. Two cell-size checkpoints are integrated into the cell cycle to maintain size homeostasis (Umen 2005). In early/mid G_1, cells pass commitment (Figure 1), a checkpoint that governs subsequent completion of the cell cycle and requires cells to attain sufficient mass for at least one cell division (Craigie and Cavalier-Smith 1982; John 1984; McAteer *et al.* 1985). Cells that have passed commitment will divide at least one time even in the absence of further growth, whereas precommitment cells stay in a resting state if growth ceases. Although it is formally analogous to Start in budding yeast, the commitment size checkpoint in Chlamydomonas does not coincide with the initiation of S phase. In fact, cells that have passed commitment remain in G_1 for an additional 5–10 hr (the delay period) and will continue to grow during the delay period if conditions permit. A second difference from yeasts is that the Chlamydomonas commitment size threshold is largely insensitive to growth rates (John 1987). Depending on culture conditions, cells in G_1 can grow as little as 2-fold or as much as 30-fold; therefore, the number of S/M cycles must be regulated to produce uniform-sized daughters. Indeed, the number of cell divisions undertaken by a mother cell is related to her size, such that larger mother cells divide more times than smaller mother cells, thus ensuring that daughter cell size distributions are largely invariant (Craigie and Cavalier-Smith 1982; Donnan and John 1983). Because S/M can occur in the absence of concurrent growth, daughter cell size can be used as a direct measure of the cell-size checkpoint that operates during S/M to control cell division numbers (Umen and Goodenough 2001; Umen 2005).

Mutations in the *MAT3* gene alter cell-size checkpoint control, resulting in a small-cell phenotype. *mat3* null mutants pass commitment at a reduced size during G_1, remain in G_1 for a normal delay period, and then undergo supernumerous divisions to produce daughters that are 25–35% the size of wild-type daughters. (Armbrust *et al.* 1995; Umen and Goodenough 2001). Previously, we showed that the Chlamydomonas homologs of E2F and DP, encoded by *E2F1* and *DP1*, respectively, are positive regulators that function downstream of MAT3/RB to control the commitment and S/M size checkpoints (Fang *et al.* 2006). *dp1* null mutations and *e2f1* dominant mutations were found to suppress the small-size phenotype of *mat3* cells by increasing the commitment size threshold and by reducing the number of divisions during S/M. Moreover, suppression of *mat3* by *dp1* and *e2f1* mutants was due to alterations in size checkpoint regulation rather than due to a lengthened or slowed cell cycle. In summary, our previous findings confirmed that the cell-cycle regulatory function and genetic wiring of the RB pathway are conserved in Chlamydomonas, making it an attractive model for further analyses.

Here we report the isolation and characterization of four new suppressors of *mat3*: *smt7-1*, *smt14-1*, *smt15-1*, and *smt16-1*. Like *dp1* and *e2f1*, these mutants suppressed *mat3* by affecting size checkpoint control. While the *smt* mutants individually were weaker suppressors than *dp1* and *e2f1*, in some double-mutant combinations they were able to suppress *mat3* as effectively as *dp1* or *e2f1*. Moreover, some of the *smt* double mutants phenocopied the large-cell phenotype of *dp1*. Complementation experiments showed that *SMT7* encodes a predicted small ubiquitin-like modifier (SUMO) peptidase. Together our data suggest the existence of a complex genetic network that functions downstream of MAT3/RB to control cell division.

MATERIALS AND METHODS

Strains and culture conditions: *C. reinhardtii* wild-type strains CC1690 (21gr, *MT+*), CC1691 (6145C, *MT−*), and *mat3-4* (Umen and Goodenough 2001) were used for all experiments and grown in either Tris–acetate–phosphate (TAP) or high-salt media (HSM) (Harris 1989) as described below. Gametes were generated by growing cells on TAP 1.5% agar plates in light for 5–8 days and resuspending the cells in nitrogen-free HSM. Mating and zygote germination were done using standard procedures (Harris 1989). For segregation and linkage analyses bulk meiotic progeny were germinated on HSM plates, resuspended in TAP, serially diluted, and replated for single colonies to obtain meiotic segregants. Individual progeny were picked

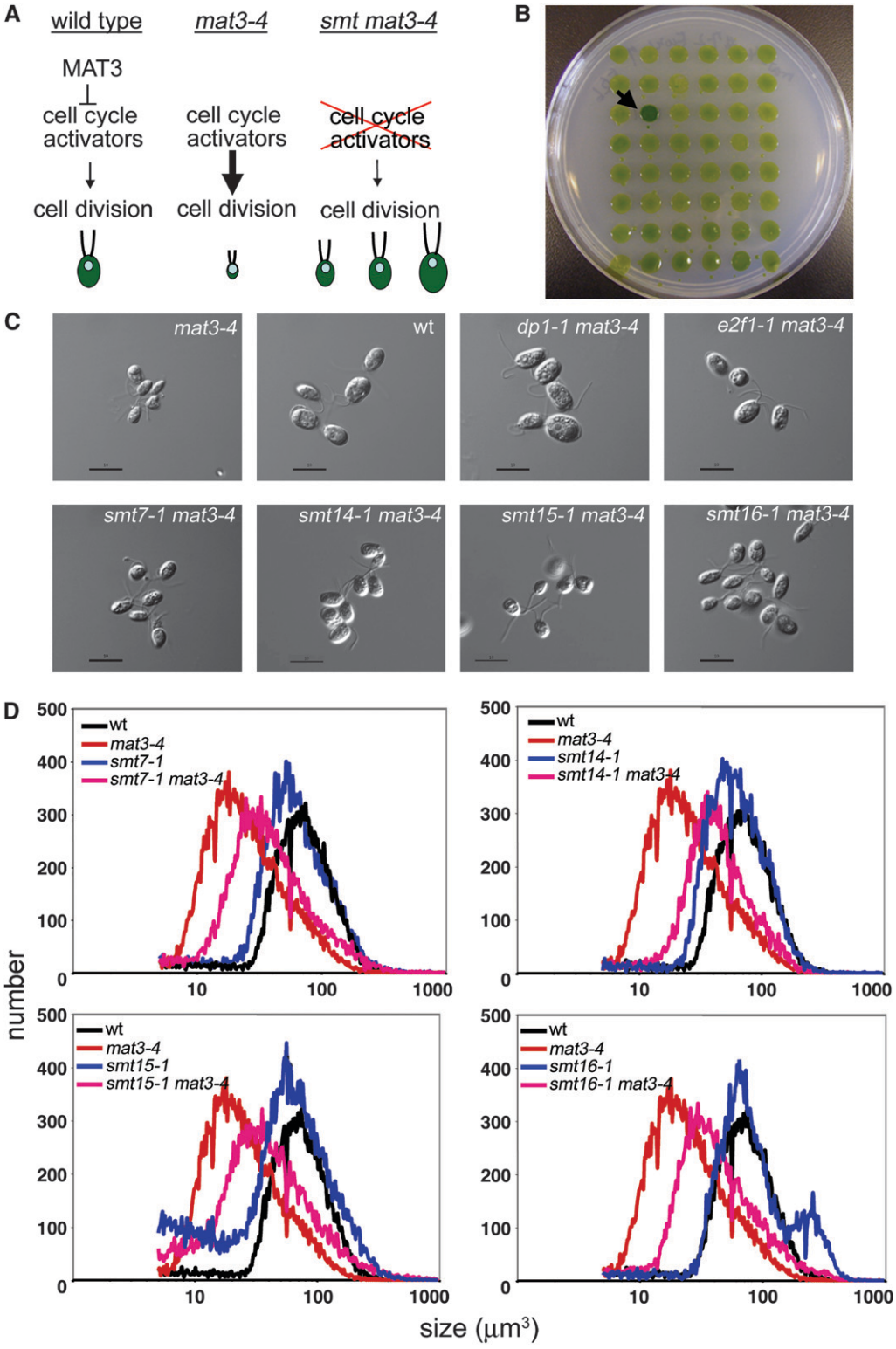

FIGURE 2.—Suppressors of *mat3-4*. (A) Conceptual representation of a suppressor screen. (B) Agar plate showing the color-based isolation of *mat3-4* suppressors. The arrow points to a suppressor strain. (C) Nomarski images of daughter cells from the indicated strains. Bar, 10 μm. (D) Cell-size distributions of dark-shifted cultures from the indicated strains. The smaller peak in the *smt16-1* sample to the right of the main peak represents unhatched daughters that remained in the mother cell wall after division.

randomly and scored for paromomycin resistance (20 μg/ml), marking the *aphVIII* insertion, or emetine resistance (60 μg/ml), marking the *mat3-4* mutation.

Insertional mutagenesis: Liquid cultures of freshly subcloned, unsuppressed *mat3-4* were grown to a density of ~10^7 cells/ml. The cells were transformed with 0.5 μg of *Not*I- or *Eco*RI-cut pSI103 plasmid (SIZOVA *et al.* 2001), using the glass bead method (KINDLE 1990). Transformants were selected on TAP plates containing 12 μg/ml paromomycin. Individual transformants were transferred into 200 μl TAP in a 96-well microtiter plate, allowed to grow for 3–4 days, and stamped onto TAP and HSM plates with a 48-prong inoculator (LabWorks, Novato, CA). After 10 days the transformants were scored for suppression of the *mat3-4* size phenotype on the basis of color (Figure 2B), and positive clones were retested for suppression of the *mat3-4* size phenotype.

TABLE 1

List of PCR mapping primers

Primer name	Primer sequences (5′–3′)	Primer name	Primer sequences (5′–3′)
SMT7-3	5′-ACGTGTTGACAGGGACGAAC-3′	SMT7-4	5′-AGGACTGGCTTTGAACAGCA-3′
SMT7-8	5′-GTGGGTGTATGCGTGCTTGT-3′	SMT7-9	5′-GAATGCATTGGTTGCAGGAG-3′
SMT7-14	5′-GTTTGGCGACAATGATTCCA-3′	SMT7-15	5′-AGCTGCTGCTTGTTCAGCAC-3′
SMT7-16	5′-ACCGGAGGGACTCAGATTCA-3′	SMT7-17	5′-CAGCACGACATGTAGCGTCA-3′
SMT7-18	5′-ATTTAATTGGTCGCGGGTTG-3′	SMT7-19	5′-AGCATGTGGGCTTAGGAGGA-3′
SMT7-20	5′-TCCGCTCCCTTCTCAGAGTC-3′	SMT7-21	5′-AGTGGTGGTTGGGGTACGAC-3′
SMT7-22	5′-CAAAGACAGGGGGTCCTGAG-3′	SMT7-23	5′-CATGTTTGGGGACATGTTGG-3′
SMT7-33	5′-AGGTTGGAGGGAGAGGAAGG-3′	SMT7-34	5′-GCTCTCACCACGCAACAGAG-3′
SMT7-35	5′-CCTTCCTCTCCCTCCAACCT-3′	SMT7-36	5′-CAATGGCCAAGCTCACACTC-3′

Determination of the *smt7-1* insertion site: A phage library was constructed from *Sau*3AI-digested *smt7-1 mat3-4* genomic DNA using λBlueSTAR-1 vector arms according to the manufacturer's instructions (EMD Chemicals, San Diego). Phage clones were screened using a radiolabeled *aphVIII* probe amplified from PSI103, using primers 5′-GATTCCCGTACCTCG TGTTGT-3′ and 5′-GTAAAACGCCAGCTTTTCCTC-3′. Positive clones were purified and the inserts were converted into plasmids for sequencing. Genomic DNA that flanked PSI103 was identified using sequencing primer 5′-GGTCATAGCT GTTTCCTGTGTG-3′ that resided in pSI103.

Isolation of the SMT7 genomic DNA fragment and complementation of *smt7-1*: Bacterial artificial chromosome clone pTQ9664 was digested with *Eco*RI and *Sac*I and a 14,364-bp fragment containing the predicted SUMO peptidase gene was gel purified and ligated to *Eco*RI- and *Bam*HI-cut pSP124 (Lumbreras *et al.* 1998) to generate pSMT7.1. pSMT7.1 was transformed into *smt7-1 mat3-4* using the glass bead method (Kindle 1990), and transformants were selected on TAP containing 5 μg/ml zeocin (Invitrogen, San Diego). Alternatively, pSMT7.1 or BAC clone pTQ15284 (containing the thioredoxin and conserved plant protein-encoding genes) were cotransformed into *smt7-1 mat3-4* with a hygromycin-resistance gene from plasmid pHyg3 (Berthold *et al.* 2002) and transformants selected on TAP containing 30 μg/ml hygromycin (Roche). Transformants were screened for smaller cell size that would be indicative of complementation. Complementation was confirmed as described in results.

RT–PCR of *SMT7*: Total RNA was isolated as previously described (Fang *et al.* 2006). Approximately 5 μg of total RNA were used for cDNA synthesis. cDNA was synthesized at 55° for 70 min, using ThermoScript RT–PCR (Invitrogen) according to the manufacturer's instructions with a mixture of dT and random primers (9:1 ratio). Nested PCR was used to amplify a portion of the *SMT7* cDNA under the following conditions: 20-μl RT–PCR reaction with 1.5 μl cDNA, 1× ExTaq buffer, 2% DMSO, 80 μm dNTPs with a 1:3 ratio of dGTP:7-deaza-dGTP (New England BioLabs, Beverly, MA), 1 μm primers, and 0.35 units ExTaq polymerase (TAKARA, Shiga, Japan). The first-round primers were 5′-GGCTGGTCGAAGTCCCAGT-3′ and 5′-AGGACCGGCAGTGTGTGCAG-3′ with amplification conditions as follows: 95° for 3 min and then 50 cycles of 95° for 30 sec, 65° for 30 sec, and 72° for 10 sec. The second-round primers were 5′-GGCTGGTCGAAGTCCCAGT-3′ and 5′-GCC AGGACAAACTCAAGACCAG-3′ with amplification conditions as follows: 95° for 3 min and then 56 cycles of 95° for 30 sec, 65° for 30 sec. The amplified cDNA was sequenced to confirm its identity. An internal control cDNA for G-protein β-subunit-like protein (GBLP) was amplified from 0.25 μl cDNA with 80 μm unmodified dNTPs, using the primers 5′-GTCATCCACTGCCTGTGCTTCT-3′ and 5′-GGCCTTCTT GCTGGTGATGTT-3′ with amplification conditions as follows: 95° for 3 min and then 36 cycles of 95° for 30 sec, 65° for 30 sec.

***smt7-1* deletion mapping and *smt* genotyping:** One microliter of genomic DNA prepared as described (http://www.chlamy.org/methods/quick_pcr.html) was used for PCR amplification. PCR fragments were amplified using Taq DNA polymerase in a final volume of 20 μl in the presence of 1× ExTaq buffer (Takara Bio), 1 μm primers, 80 μm dNTP, and 2% DMSO. Primer pairs used for PCR-based genotyping are listed in Table 1. PCR conditions were as follows: 96° for 2 min and then 42 cycles of 94° for 30 sec, 65° for 30 sec, 72° for 45 sec. For specific *smt* strains, the genotyping primers are as follows: 5′-CATCATTGCGAGTTGCCATT-3′ and 5′-GGTCATAGCTG TTTCCTGTGTG-3′ for *smt7-1*, 5′-TGGCTAAGCCGTCTTCT TGT-3′ and 5′-CGATTTCGGCCTATTGGTTA-3′ for *smt14-1*, 5′-ACGGTATGTGTCGCAATCCT-3′ and 5′-CGATTTCGGC CTATTGGTTA-3′ for *smt15-1*, 5′-AAGCAGCTCGAGGAGCT CAA-3′ and 5′-CGATTTCGGCCTATTGGTTA-3′ for *smt16-1*, and 5′-GGGACACCCCTTACGTATCC-3′ and 5′-CACAACAA CCCACTCACAACC-3′ for *mat3-5*.

The *dp1-1* mutation was genotyped by Southern blotting as described previously (Bisova *et al.* 2005), using an *aphVIII* DNA probe (see above).

Vegetative diploid construction: First, *smt7-1 mat3-5 MT–*, *smt14-1 mat3-5 MT–*, *smt15-1 mat3-5 MT–*, and *smt16-1 mat3-5 MT–* strains were generated from a cross of each *smt* single mutant to *mat3-5* (*MT– mat3* mutation). Strain genotypes were confirmed by PCR as described above. *smt7-1 mat3-5*, *smt14-1 mat3-5*, *smt15-1 mat3-5*, and *smt16-1 mat3-5* were then mated to a *SMT mat3-4 MT+* strain and vegetative diploids were selected on TAP agar containing 12 μg/ml paromomycin and 50 μg/ml emetine. Vegetative diploids with the genotypes *mat3-4/mat3-5*, *SMT7/smt7-1 mat3-4/mat3-5*, *SMT14/smt14-1 mat3-4/mat3-5*, *SMT15/smt15-1 mat3-4/mat3-5*, and *SMT16/smt16-1 mat3-4/mat3-5* were tested by PCR to confirm the presence of both mating types (Zamora *et al.* 2004) and of both wild-type and mutant alleles of the *SMT* gene.

Dark-shift experiments and cell-size measurements: Liquid cultures were grown in continuous light and cell density was maintained between 10^5 and 10^6 cells/ml in HSM before dark incubation. Cultures were then incubated in the dark for 16–18 hr. Cell-size distributions of light-grown cultures were measured to ensure that the majority of cells were above commitment size before dark incubation that the majority of them would divide and produce daughters. After dark shifting cells were fixed with 0.2% glutaraldehyde, and Tween 20 was added to a final concentration of 0.005% to prevent cells from sticking to the wall of the tube. Cell-size distributions were measured using a Coulter Counter (MULTISIZER 3; Beckman–Coulter, Miami) set to count at least 300 events in the modal channel. After counting, the histogram curves were smoothed

using the Multisizer software and the modal size was determined from the position of the maximum peak height of the smoothened curve. The smoothening did not alter the shape of the histogram curve, but served to mitigate against random fluctuations in the modal channel that added noise to the data. Modal cell size was thus measured from at least three independent cultures and averaged to determine the modal daughter cell size. Standard experimental error was calculated for all measurements and average modal size differences that were larger than the combined error terms were considered significant. Modal (and not mean or median) size was used in these experiments because it proved to be relatively insensitive to the fraction of cells in the population that were in a precommitment state prior to dark shifting. These precommitment cells were larger than newly formed daughters and could skew the mean and median population sizes in dark-shifted populations, but were empirically found to exert less effect on modal size measurements.

Growth rate and commitment analyses: Asynchronous liquid cultures were grown in continuous light and cell density was maintained between 10^5 and 10^6 cells/ml by dilution into fresh HSM. Cultures at ~1–3 × 10^5 cells/ml were used for the initial sampling point and additional samples were collected every 3 hr for 12 hr. Growth (mass doubling time) was measured by determining the chlorophyll content of cultures at each time point as previously described (Harris 1989), and each growth experiment was repeated at least three times. Commitment was measured by dark shifting continuous-light cultures to induce partial synchrony and then returning the cultures to continuous light where passage through commitment was assayed as previously described (Umen and Goodenough 2001; Fang *et al.* 2006).

RESULTS

Screen for suppressors of *mat3*: RB/MAT3 is a negative cell-cycle regulator whose absence causes premature cell-cycle activation and supernumerous cell divisions, presumably due to inappropriate activation of E2F1-DP1 (Fang *et al.* 2006) and other downstream targets. We reasoned that mutations in such targets would suppress the small-size phenotype of *mat3* mutants (Figure 2A) and the screen might, therefore, reveal cell-cycle regulators whose activity is rate limiting in the absence of MAT3. Insertional mutagenesis with a paromomycin resistance-conferring plasmid (Sizova *et al.* 2001) was used to screen for bypass suppressors of a *MAT3* null allele, *mat3-4* (Umen and Goodenough 2001). We have routinely observed that *mat3* mutant cells are sensitive to starvation and therefore lose viability and turn yellow on agar plates. We took advantage of the fact that suppressors of *mat3* produce colonies that are less sensitive to starvation and are darker green than colonies of unsuppressed cells (Armbrust *et al.* 1995; Figure 2B). A total of 20,500 paromomycin-resistant transformants of *mat3-4* were screened for darker color, and after phenotypic confirmation and retesting we obtained 19 *s*uppressors of ***mat3*** (*smt* mutants) that increased the size of *mat3-4* cells by varying degrees.

Twelve of the *smt* mutants produced cells that were larger than wild type (Figure 2C). They were found to have insertions in the *DP1* locus (Fang *et al.* 2006). Three of the *smt* mutants produced cells that were similar in size to wild type (Figure 2C). These *smt* mutants were found to have insertions in the *E2F1* gene that caused a dominant suppression phenotype (Fang *et al.* 2006). While the basis for dominant suppression is not known, all of the *E2F1* suppressor alleles had insertions in the 3′ part of the gene, suggesting that this region is a "hot spot" for mutations.

Four additional mutants—*smt7-1*, *smt14-1*, *smt15-1*, and *smt16-1*—produced cells that were larger than those of the parental *mat3-4* strain but smaller than wild type (Figure 2, C and D). The characterization of these four suppressors is reported below and they are simply referred to as *smt* mutants (*smt*s).

Linkage and segregation analysis: We tested whether the *smt* suppression phenotype cosegregated with the inserted *aphVIII* transgene that conferred paromomycin resistance (paroR) by crossing *smt7-1 mat3-4*, *smt14-1 mat3-4*, *smt15-1 mat3-4*, or *smt16-1 mat3-4* to a wild-type stain (6145c *MT*−) and examining randomly selected progeny whose *mat3-4* mutation was scored by emetine resistance (emR). Paromomycin-sensitive, emetine-resistant (paroS, emR) and paromomycin-resistant, emetine-resistant (paroR, emR) progeny were collected and their size distributions were compared. In each case, the size distribution of the paroR emR segregants was slightly larger than that of the paroS emR segregants that contained only the *mat3-4* mutation (Table 2 and data not shown). From this result we concluded that the suppression phenotype for each *smt* mutation was linked to the inserted *aphVIII* transgene.

To further verify linkage between the *aphVIII* (paroR) transgene insertion and suppression of *mat3-4*, we identified paroR emS segregants from the above cross that contained only the *smt* mutation and were wild type for *MAT3*. These strains were crossed to a freshly subcloned *mat3-4* isolate and the resulting paroS emR and paroR emR progeny were compared. Again, in each case the paroR emR double-mutant progeny were always slightly larger than the paroS emR progeny that contained only the *mat3-4* mutation (Figure 3 and Table 3). These experiments confirmed our conclusion that the *aphVIII* insertion was linked to *mat3* suppression for each *smt* mutant.

Having established linkage between the *aphVIII* insertion and suppression of *mat3-4*, we then asked whether any of the *smt* mutants were linked to each other. Linkage between the *smt* mutants was determined by pairwise crossing each *smt* mutant to the others and scoring for wild-type recombinants that would be paroS and expected to comprise approximately one-quarter of the progeny if the two loci were unlinked. Each of the *smt* × *smt* crosses produced at least 23% wild-type (paroS) progeny, indicating that none of the *smt*s are linked (Table 4). The overrepresentation of wild-type recombinants (>25%) in crosses involving *smt15-1* may be due to

TABLE 2

Linkage of paromomycin resistance and size suppression of *mat3* from crosses using original *smt* mutant isolates

	Genetic markers				
	Inferred genotype, *mat3-4* suppression		Inferred genotype		
Cross	paroR emR: *smt mat3-4*, suppressed:unsuppressed	paroS emR: *SMT mat3-4*, suppressed:unsuppressed	paroS emS: *SMT MAT3*	paroR emS: *smt MAT3*	Total scored
dp1-1 mat3-4 MT+ × wt *MT*−	5:0	0:7	5	7	24
e2f1-1 mat3-4 MT+ × wt MT−	11:0	0:8	19	10	48
smt7-1 mat3-4 MT+ × wt *MT*−	3:0	0:8	8	5	24
smt14-1 mat3-4 MT+ × wt *MT*−	6:0	0:2	8	7	24
smt15-1 mat3-4 MT+ × wt *MT*−	4:0	0:6	9	5	24
smt16-1 mat3-4 MT+ × wt *MT*−	7:0	0:5	5	7	24

ParoR, paromomycin resistant; paroS, paromomycin sensitive; emR, emetine resistant (*mat3-4*); emS, emetine sensitive (*MAT3*). Suppressed:unsuppressed indicates the number of progeny with the indicated genetic markers that showed a suppressed *vs.* unsuppressed *mat3-4* size phenotype.

growth defects that caused *smt15-1* progeny to be outcompeted by wild-type progeny during the short postmeiotic growth period that preceded subcloning (see MATERIALS AND METHODS).

Dominance testing of *smt* mutants: To determine whether *smt* mutants were dominant or recessive we constructed vegetative diploids for each strain and assessed their size distributions as we did previously for assessing the dominance of *e2f1* mutations (FANG *et al.* 2006) (see MATERIALS AND METHODS). In each case the heterozygous *smt/SMT mat3-4/mat3-5* strain had a size distribution that was similar to that of the control strain (*SMT/SMT mat3-4/mat3-5*), indicating that *smt7-1*, *smt14-1*, *smt15-1*, and *smt16-1* were recessive alleles and probably represented loss-of-function mutations (Figure 4 and Table 5).

Cell-size checkpoint alterations in *smt* mutants: *Daughter cell size:* We used dark-shift experiments to differentiate two possible mechanisms of *mat3* size suppression by the *smt* mutants: (i) slowed cell-cycle progression or (ii) altered size checkpoint control. If the *smt*s suppressed *mat3* by the first mechanism, they would progress through the cell cycle more slowly than the *mat3* strain but produce daughters that were similar in size to unsuppressed *mat3*. On the other hand, if suppression were caused by an altered size checkpoint mechanism, then the suppressed strains would produce daughters larger than *mat3-4* even when given a long period of time in the dark in which to divide (FANG *et al.* 2006). Cultures of control *mat3-4* cells along with *smt mat3-4* suppressed strains were grown in continuous light to generate cells randomly distributed throughout the cell

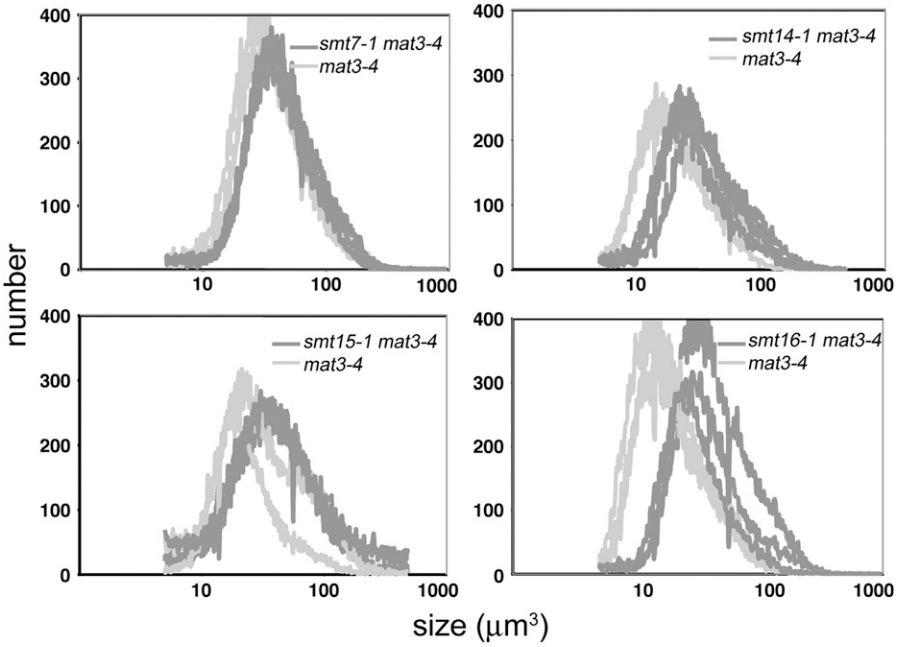

FIGURE 3.—Cosegregation of pSI103 insertion and *smt* phenotype. Cell-size distributions from dark-shifted cultures of *mat3-4* (paromomycin-sensitive, emetine-resistant) or *smt mat3-4* (paromomycin-resistant, emetine-resistant) progeny from crosses between each *smt* single mutant and *mat3-4* are shown. Three progeny of each genotype are overlaid in each graph. See RESULTS for details.

TABLE 3

Linkage of paromomycin resistance and size suppression of *mat3* from outcrossed *smt* strains

Cross	Genetic markers: Inferred genotype, *mat3-4* suppression: paroR emR: *smt mat3-4*, suppressed:unsuppressed	Inferred genotype, *mat3-4* suppression: paroS emR: *SMT mat3-4*, suppressed:unsuppressed	Inferred genotype: paroS emS: *SMT MAT3*	Inferred genotype: paroR emS: *smt MAT3*	Total scored
mat3-4 MT+ × *smt7-1 MT−*	4:0	0:3	15	10	32
mat3-4 MT+ × *smt14-1 MT−*	11:0	0:3	3	7	24
mat3-4 MT+ × *smt15-1 MT−*	4:0	0:6	10	4	24
mat3-4 MT+ × *smt16-1 MT−*	7:0	0:5	5	7	24

ParoR, paromomycin resistant; paroS, paromomycin sensitive; emR, emetine resistant (*mat3-4*); emS, emetine sensitive (*MAT3*). Suppressed:unsuppressed indicates the number of progeny with the indicated genetic markers that showed a suppressed *vs.* unsuppressed *mat3-4* size phenotype.

cycle and then shifted into the dark for 16–18 hr. Upon shifting to the dark, growth ceases and cells that have passed commitment enter S/M phase (typically within 5–10 hr for *mat3-4*) and divide to produce daughter cells. After dark incubation, suppressor strains produced daughters whose sizes were slightly larger than *mat3-4* control strains (Table 6 and data not shown). These results indicated that suppression of *mat3-4* by *smt7-1*, *smt14-1*, *smt15-1*, and *smt16-1* involves an alteration of the S phase/mitotic size checkpoint function that regulates daughter cell size.

We also used the dark-shift assay to test whether *smt* mutants had cell-size and cell-cycle defects as single mutants when segregated away from *mat3-4* into a wild-type *MAT3* background. *smt7-1*, *smt14-1*, and *smt16-1* strains produced daughter cells that were similar in size to wild type after dark shifting (Table 6). Unexpectedly, the *smt15-1* single mutant generated daughters that were slightly smaller than wild type after dark incubation (Table 6). Moreover, *smt15-1* was the only *smt* that had a significant growth defect with an average mass doubling time of 8.3 hr *vs.* 5.1 hr for wild type (Table 6). It is important to note that mass doubling time was measured in asynchronous continuous-light culture conditions and was not directly correlated with overall cell-cycle timing that was similar for wild type and all the *smt* mutants. The lack of correlation between mass doubling time and cell-cycle time is due to the nature of the multiple-fission cell cycle (Figure 1), where variable amounts of growth can be easily accommodated within one cycle.

TABLE 4

Linkage analysis of the *smt* mutants

Cross	Paromomycin-resistant colonies	Paromomycin-sensitive colonies	Total scored colonies
smt7-1 × *smt14-1*	21	11	32
smt7-1 × *smt15-1*	18	6	24
smt7-1 × *smt16-1*	37	11	48
smt14-1 × *smt16-1*	24	8	32
smt15-1 × *smt16-1*	22	10	32
smt15-1 × *smt14-1*	21	11	32

Commitment cell size: Commitment is an early/mid-G_1 size checkpoint controlled by the MAT3/RB pathway in Chlamydomonas. Since *mat3-4* cells were previously shown to pass commitment at a reduced cell size compared to wild type (Umen and Goodenough 2001), we asked whether *smt7-1*, *smt14-1*, *smt15-1*, or *smt16-1* altered the commitment cell size threshold of *mat3-4* mutants. Ideally, commitment is measured in highly synchronous cultures. However, neither *mat3-4* nor any of the *smt mat3-4* double mutants could be synchronized to a high degree. Therefore, we determined the commitment size threshold of the suppressed strains, using partially synchronized cultures as was done previously for *mat3-4* (Umen and Goodenough 2001; Fang *et al.* 2006). For *mat3-4* cultures, cells passed commitment as they approached ~100 μm^3, a value comparable to previous measurements (Umen and Goodenough 2001 and Table 6). In contrast, the *smt7-1 mat3-4*, *smt14-1 mat3-4*, *smt15-1 mat3-4*, and *smt16 mat3-4* strains all passed commitment at larger sizes than *mat3-4* (Table 6) but at smaller sizes than wild-type cells (~200 μm^3). These results showed that mutations in *smt*s partially suppressed the commitment cell-size checkpoint defect of *mat3-4*. Therefore, like the *dp1* and *e2f1* mutants, the *smt*s suppressed both the daughter cell-size and the commitment cell-size checkpoints of *mat3-4* cells.

We used the same commitment assay to investigate whether *smt7-1*, *smt14-1*, *smt15-1*, or *smt16-1* single mutants affected commitment size when segregated away from *mat3-4*. *smt14-1* cells had a commitment size that was similar to that of wild type while *smt16-1* cells passed commitment at a larger size (~230 μm^3) (Table 6). *smt7-1* mutant cells did not behave consistently in the commitment assay, often passing commitment at a size that was larger than that of wild type, but not always. The unstable commitment behavior we observed for *smt7-1* was similar to that observed previously for *e2f1-1* (Fang

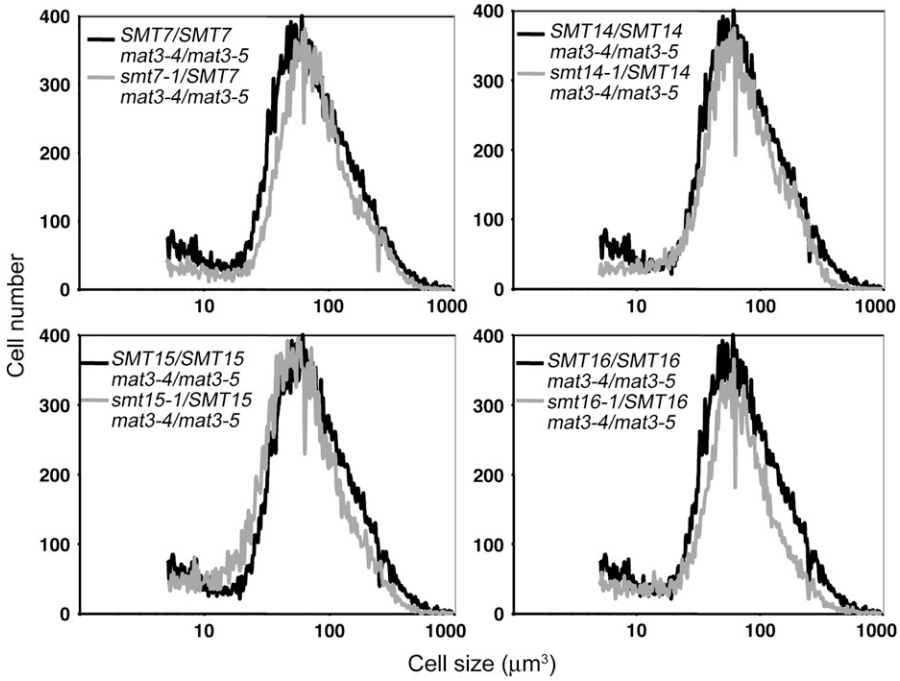

FIGURE 4.—Dominance testing of *smt* mutants. Size distributions of dark-shifted vegetative diploids of the indicated genotype are shown.

et al. 2006) and suggested that the ability of *smt7-1* strains to couple cell size to passage through commitment was partially compromised. However, as described above, once *smt7-1* and *smt16-1* cells passed commitment, they could divide to produce daughter cells of wild-type size, indicating that their daughter cell-size checkpoint was intact. In contrast to the other *smt*s, *smt15-1* cells were found to reach commitment at a slightly smaller size than that of wild type (~160 μm³ *vs.* ~200 μm³), mirroring the result we obtained for *smt15-1* when assayed for daughter cell size (see above). The size checkpoint phenotypes of the *smt15-1* single mutant suggested that *SMT15* encodes a negative cell-cycle regulator like *MAT3*, yet a recessive allele, *smt15-1*, suppressed (rather than enhanced) the *mat3-4* size phenotype. Possible explanations for the paradoxical behavior of *smt15-1* are elaborated in the DISCUSSION.

Genetic interactions between smt mutations and dp1: Previously we showed that *E2F1* and *DP1* are major downstream targets in our *mat3* suppressor screen (FANG *et al.* 2006). We wanted to determine whether the *smt* mutants acted independently of E2F1/DP1 or were in the same pathway. If they acted independently of E2F1/DP1, then they would be expected to enhance the size phenotype of *dp1* mutants or to display synthetic viability phenotypes in combination with *dp1* mutations. Conversely, the lack of such interactions would suggest that the *smt*s were affecting the same pathway as *dp1*, perhaps as downstream effectors or as modulators of E2F1-DP1 activity. To test for genetic interactions between *smt*s and a canonical positive regulator of the RB pathway, a *DP1* null allele, *dp1-1*, was crossed to each *smt mat3-4* strain and both double-mutant (*smt dp1-1*) and triple-mutant (*smt dp1-1 mat3-4*) progeny were recovered. In all cases, mutant progeny were produced in approximately the expected ratios (except for slightly reduced recovery of *smt15-1* combinations that was probably due to slow growth as described above), indicating that none of the *smt*s was synthetically lethal or slow growing when combined with *dp1-1*. Moreover, in no case was the cell-size phenotype of an *smt dp1-1* double mutant greater than that of the *dp1-1* single mutant (Figure 5 and data not shown). The absence of genetic interactions with *dp1-1* suggests that the SMTs might act as targets or effectors of E2F1-DP1 activity, but do not contribute to cell-cycle regulation independently of E2F1-DP1.

TABLE 5

Dominance testing of the *smt* mutants

Vegetative diploid genotype	Daughter cell size (μm³)
mat3-4/mat3-5	64 ± 3.1
smt7-1 mat3-4/SMT7 mat3-5	61 ± 3.4
smt14-1 mat3-4/SMT14 mat3-5	65 ± 2.0
smt15-1 mat3-4/SMT15 mat3-5	58 ± 1.7
smt16-1 mat3-4/SMT 16 mat3-5	60 ± 2.6

Standard errors were derived from three independent cultures.

Genetic interactions among the smt mutants: The mild suppression of *mat3-4* caused by *smt* mutants and their relatively weak or absent cell-cycle phenotypes as single mutants suggested that the *SMT* loci encoded functions that were partially redundant and could be revealed only when the RB/MAT3 pathway was disrupted. To better understand their suppressor phenotypes and their relationships to each other we generated double-mutant combinations between all the *smt*s in the pres-

TABLE 6

Growth rate, daughter size, and commitment size for the indicated strains

Genotype	Daughter cell size (μm^3)	Commitment size (μm^3)	Doubling time (hr)
Wild type	65 ± 2.7	200 ± 5	5.1 ± 0.3
smt7-1	65 ± 2.9	≥200[a]	5.4 ± 0.3
smt14-1	66 ± 4.1	211 ± 11	5.3 ± 0.3
smt15-1	51 ± 4.1	159 ± 11	8.3 ± 0.5
smt16-1	66 ± 6.1	230 ± 11	5.3 ± 0.4
mat3-4	21 ± 1.4	103 ± 10	7.3 ± 0.2
smt7-1 mat3-4	37 ± 1.4	150 ± 22	6.8 ± 0.2
smt14-1 mat3-4	30 ± 1.6	151 ± 10	6.4 ± 0.2
smt15-1 mat3-4	37 ± 2.1	179 ± 13	9.7 ± 0.6
smt16-1 mat3-4	28 ± 1.2	126 ± 22	7.4 ± 0.3

Standard errors for doubling time, daughter cell size, and commitment size were derived from at least three independent cultures. For commitment size threshold determination standard errors were derived from multiple time points in each of three independent experiments.

[a] The *smt7-1* commitment size could not be accurately determined, but was at least as large as that of wild type. See RESULTS for details.

ence or absence of a *mat3-4* mutation and measured the size distributions of dark-shifted daughter cells (Table 7). These higher-order mutant combinations revealed a complex pattern of genetic interactions between different *smt*s and *mat3*. Several of the *smt*s showed synergistic suppression of *mat3-4*: *smt7-1 smt15-1 mat3-4*, *smt7-1 smt16-1 mat3-4*, and *smt15-1 smt16-1 mat3-4* all showed very strong additive effects, suppressing *mat3-4* to wild-type size or larger (Figure 6 and Table 7). However, other mutant combinations that included *smt14-1* (*smt7-1 smt14-1 mat3-4*, *smt14-1 smt15-1 mat3-4*, and *smt14-1 smt16-1 mat3-4*) showed weakly additive or no additive suppression of *mat3-4* (Table 7).

When the double-mutant *smt* combinations were analyzed in the absence of *mat3-4*, additional interactions emerged. Strikingly, the *smt7-1 smt15-1*, *smt7-1 smt16-1*, and *smt15-1 smt16-1* combinations all caused a synthetic large-cell phenotype that was nearly as severe as that of *dp1* null mutations (Figure 6 and Table 7). In the case of *smt7-1 smt15-1* the synthetic large-cell phenotype occurred regardless of whether the *MAT3* locus was wild type or mutant. On the other hand, the synthetic large-cell phenotypes of *smt7-1 smt16-1* and *smt15-1 smt16-1* were partially counteracted by the *mat3-4* mutation, leading to the production of daughters of approximately wild-type size (Figure 6 and Table 7). The synthetic large-cell phenotypes involving *smt15* were particularly interesting since by itself *smt15-1* was found to have a slight small-cell phenotype. Unlike its interactions with either *smt7-1* or *smt16-1* that resulted in enhanced suppression of *mat3-4* and increased cell size, *smt15-1* displayed an epistatic interaction with *smt14-1*: *smt14-1 smt15-1* double mutants had the slightly small-cell phenotype characteristic of the *smt15-1* single mutant. Finally, the double-mutant combinations of *smt7-1 smt14-1* and *smt14-1 smt16-1* showed no genetic interactions, producing daughters that were comparable in size to each single mutant and to wild type.

In summary, three of the *smt* mutants—*smt7-1*, *smt15-1*, and *smt16-1*—showed strong synergistic interactions in various combinations with each other and with *mat3-4*, whereas *smt14-1* showed little or no syn-

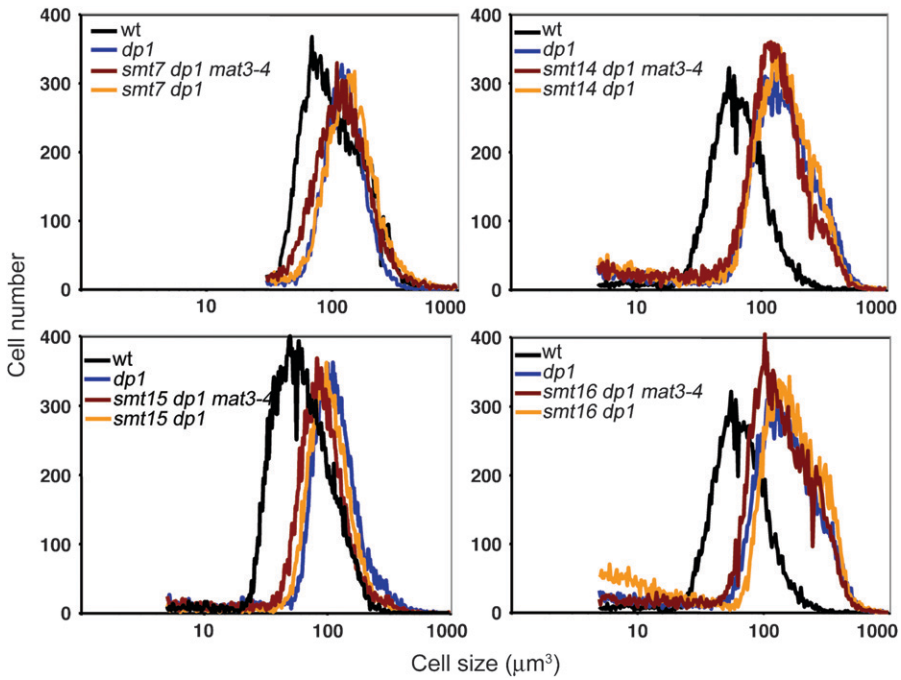

FIGURE 5.—Test for genetic interactions between *dp1-1* and *smt* mutants. Cell-size distributions of dark-shifted cultures from indicated genotypes are shown.

TABLE 7

Daughter cell size of indicated strain after dark shift

Genotype	Daughter cell size (μm^3)
smt7-1 smt15-1	94 ± 0.6
smt7-1 smt15-1 mat3-4	92 ± 5.6
smt7-1 smt16-1	88 ± 5.7
smt7-1 smt16-1 mat3-4	64 ± 4.1
smt15-1 smt16-1	104 ± 3.6
smt15-1 smt16-1 mat3-4	66 ± 4.6
sm7-1 smt14-1	66 ± 4.6
smt7-1 smt14-1 mat3-4	35 ± 0.9
smt14-1 smt15-1	50 ± 4.5
smt14-1 smt15-1 mat3-4	41 ± 1.5
smt14-1 smt16-1	74 ± 4.1
smt14-1 smt16-1 mat3-4	39 ± 1.5
dp1-1[a]	100 ± 3.5
dp1-1 mat3-4[a]	90 ± 2.3

Standard errors were derived from three independent cultures from at least two independent strains.

[a] Data from Fang *et al.* (2006).

ergy/additivity with the other *smt*s. Moreover, the identification of strong cell-size phenotypes for some *smt* double-mutant combinations, even when the canonical RB pathway was intact, provided independent confirmation that these *SMT* loci encode *bona fide* cell-cycle regulators. The complex set of interactions uncovered by these experiments further suggested that the SMTs function downstream of MAT3 in different pathways to effect cell-cycle entry.

Molecular characterization of smts: Southern blotting was used to examine the nature of the pSI103 plasmid insertion for each *smt* strain. *smt7-1*, *smt14-1*, *and smt15-1* were found to have a single copy of the inserted *aphVIII* transgene whereas *smt16-1* was found to have two copies of the *aphVIII* transgene inserted in tandem, which always cosegregated (Figure 7A and data not shown). The *smt7-1* mutation was followed up in more detail, and characterization of the remaining *smt*s will be described elsewhere.

The genomic DNA flanking the *smt7-1* insertion was isolated by constructing a λ-phage DNA library from *smt7-1 mat3-4* and screening for inserts that contained *aphVIII* sequences. Positive clones were further analyzed by sequencing to identify junction fragments that contained genomic DNA adjacent to pSI103 sequences (see materials and methods). Since insertional mutations are sometimes accompanied by deletions, we designed primers to amplify short segments of genomic DNA flanking the insertion region of *smt7-1* to ascertain whether these flanking regions were present. By this method we determined that *smt7-1* had ~19 kb of genomic sequence deleted from around the site of the pSI103 insertion (Figure 7B). The deleted region of *smt7-1* encompasses three gene models, including a SUMO-specific peptidase, a conserved plant protein of unknown function, and a thioredoxin-related protein.

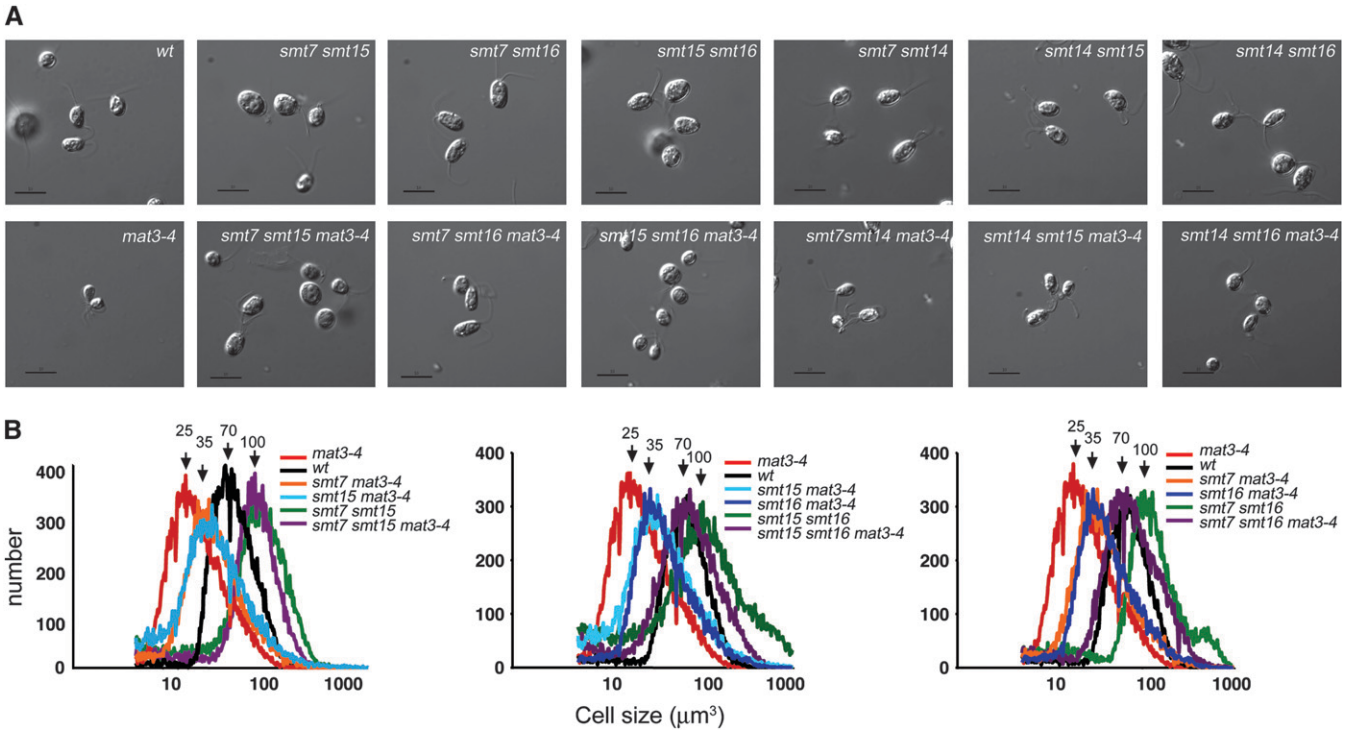

Figure 6.—Genetic interactions between *smt7-1*, *smt14-1*, *smt15-1*, and *smt16-1* mutants. (A) Nomarski images of daughter cells from indicated strains. Bar, 10 μm. (B) Cell-size distributions of dark-shifted cultures from indicated strains. Arrows indicate the approximate positions of modal peaks for the different curves.

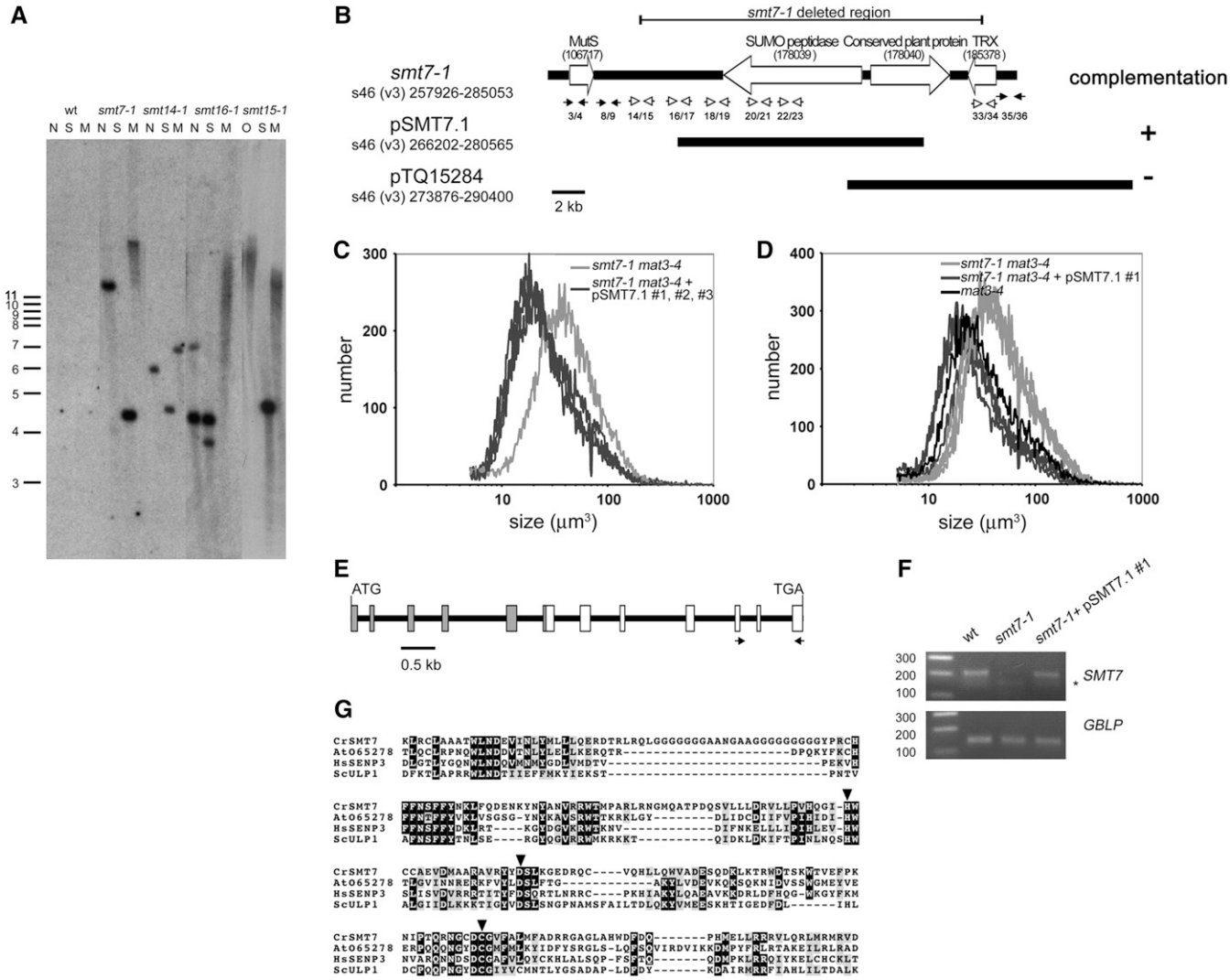

FIGURE 7.—Southern blot of *smt* insertions and complementation of *smt7-1.* (A) Southern blot of genomic DNA from indicated *smt* mutants digested with *Nhe*I (N), *Not*I (O), *Sac*I (S), or *Sma*I (M) and probed with *aphVIII* DNA. Positions and sizes of markers in kilobase units are on the left. (B) Schematic of the *smt7-1* deletion with scaffold number, genome version, and scaffold coordinates indicated. Potential gene models and intergenic regions are denoted by large open arrows and solid bars, respectively. Protein ID numbers associated with each model are in parentheses below the description. TRX, thioredoxin-related protein. The pairs of arrows below each scaffold depict the positions of PCR primers that were used to assess the structure of the *smt7-1* deletion. Open arrows indicate primer pairs that could amplify wild-type but not mutant DNA, and solid arrows indicate primer pairs that could amplify both mutant and wild-type DNA. Primer sequences are in Table 1. Results of complementation with two different constructs are shown below the schematic. (C) Size distributions of dark-shifted cells from *smt7-1 mat3-4* and three independently generated *smt7-1 mat3-4* transformants that were complemented with pSMT7.1 (#1, #2, and #3). (D) Cosegregation of pSMT7.1 and loss of *mat3-4* suppression by *smt7-1.* Size distributions of dark-shifted *smt7-1 mat3-4* and *smt7-1 mat3-4* pSMT7.1 segregants (from *smt7-1 mat3-4* pSMT7.1 #1 × wild type) compared with *mat3-4* are shown. Three progeny of each relevant genotype are overlayed in each graph. (E) Predicted *SMT7* gene model. Open boxes indicate exons confirmed by RT–PCR and shaded boxes indicate predicted exons. The locations of RT–PCR primers used to assess expression of *SMT7* in complemented strains are depicted by the arrows. (F) RT–PCR of *SMT7* or internal control message *GBLP* in the indicated strains. The asterisk denotes a nonspecific PCR product. The primer locations used to amplify *SMT7* are shown in E. (G) ClustalW alignment of SUMO peptidase domains from Chlamydomonas SMT7 (EU367939; residues 6–235 translated from partial cDNA), Arabidopsis At065728 (AAC13629, residues 39–233), human SENP3 (Q9H4L4, residues 392–573), and budding yeast Ulp1 (Q02724, residues 439–621). Inverted triangles are positioned over the residues that compose the catalytic triad.

Complementation of smt7-1: Complementation was used to determine which of the deleted genes in *smt7-1* was responsible for suppression of *mat3-4.* A *smt7-1 mat3-4* strain was transformed with a genomic construct containing either the wild-type SUMO-specific peptidase gene (pSMT7.1) or a small BAC clone (pTQ15284) containing the genes that encode both the conserved plant protein and thioredoxin-related protein as described above (Figure 7B). In several independent experiments, transformants that received the pSMT7.1

TABLE 8

Size distribution of the given genotype derived from *smt7-1 mat3-4* pSMT7.1 × wt

Genotype	Daughter cell size (μm^3)
smt7-1 mat3-4	34.3 ± 1.4
smt7-1 mat3-4 pSMT7.1	21.8 ± 1.8

Standard errors were derived from four independent *smt7-1 mat3-4* strains and five independent *smt7-1 mat3-4* pSMT7.1 strains.

construct were recovered that had lost suppression of *mat3-4*, indicating that the *smt7-1* mutation had been complemented (Figure 7C). In contrast, none of the transformants that received the pTQ15284 construct displayed complementation (data not shown). The complemented strains (*mat3-4 smt7-1* pSMT7.1) were then crossed to a wild-type strain to confirm that suppression was linked to the presence of the pSMT7.1 construct and to generate complemented *smt7-1* strains that did not contain the *mat3-4* mutation. All the *smt7-1 mat3-4* progeny that received pSMT7.1 had *mat3-4*-like cell size distributions, meaning that they were complemented, whereas all those that did not receive pSMT7.1 were suppressed like the original *mat3-4 smt7-1* strain (Figure 7D and Table 8).

We next used RT–PCR to confirm that expression of the SUMO peptidase-encoding gene was restored in complemented *smt7-1* strains (Figure 7, E and F, and data not shown). These experiments confirmed that this was the case and also revealed that the mRNA for this gene is extremely low in abundance and/or difficult to amplify since two rounds of nested amplification were required for its detection (see MATERIALS AND METHODS). We also compared *SMT7* mRNA abundance in a wild-type and a *mat3-4* strain and found no difference between the two, suggesting that the *SMT7* gene is not a transcriptional target of the RB pathway (data not shown). Taken together, these data confirmed that loss of the gene encoding a putative SUMO-specific peptidase in *smt7-1* strains is responsible for suppression of the uncontrolled cell division in *mat3-4* strains.

The gene model that corresponds to *SMT7* in version 3 of the Chlamydomonas genome (protein ID no. 178039) contains an internal gap region. We utilized newly available sequence information from the version 4 Chlamydomonas genome assembly to fill in this gap region and we also verified seven of the *SMT7* exons that encompass the SUMO peptidase domain by RT–PCR (Figure 7E, data not shown). While the N-terminal region did not show significant homology to any known proteins, sequence alignments and domain searching confirmed that the SMT7 C-terminal domain belongs to the SUMO peptidase gene family (pfam 02902) and contains the key catalytic residues that are found in this group of cysteine proteases (Figure 7G).

DISCUSSION

***smt* mutants identify new loci that contribute to RB/MAT3-mediated cell-cycle activation:** While genetic screens have previously been performed on the RB–E2F pathway in flies and worms (LU and HORVITZ 1998; STAEHLING-HAMPTON *et al.* 1999; CEOL and HORVITZ 2001; FAY *et al.* 2002; BENDER *et al.* 2004, 2007; CUI *et al.* 2004, 2006; ANDERSEN *et al.* 2006; KORENJAK and BREHM 2006; CERON *et al.* 2007; OUELLET and ROY 2007; REDDIEN *et al.* 2007), the work reported here represents, to our knowledge, the first unbiased suppressor screen using an *RB* mutant. As discussed below, the types of interactions suggest that even in a simple unicellular organism like Chlamydomonas the RB–E2F pathway appears to have a surprisingly complex output.

Previously we found that insertions in the *DP1* and *E2F1* loci were the strongest and most abundant *mat3* suppressors. Identifying these two loci as downstream effectors of RB/MAT3 confirmed that the canonical RB/E2F pathway is conserved in Chlamydomonas and also validated our screening procedure. Because the newly identified *smt*s were weaker suppressors than *dp1* and *e2f1* they were more difficult to identify, but they had a clear and measurable effect on RB/MAT3-mediated cell-size and cell-cycle control. Moreover, the fact that none of the four new suppressors were allelic suggests that our screen was not saturated and that there are more *smt* loci yet to be identified.

Three of the weak *smt*s (*smt7-1*, *smt14-1*, and *smt16-1*) had no phenotype or a very subtle cell-size or cell-cycle phenotype as single mutants, and one of them, *smt15-1*, had a phenotype that was opposite to that predicted for a downstream effector of MAT3/RB, causing a slight small-cell phenotype. Thus, the use of a sensitized genetic background for this screen revealed mutants or novel phenotypes that would not have been easily identified in a wild-type background.

The slightly small-size phenotype of the *smt15-1* single mutant was puzzling because this allele caused *mat3-4* cells to become larger. Moreover, *smt15-1* interacted synergistically with *smt7-1* and *smt16-1* to cause a large-cell phenotype (Table 7, Figure 6). A possible explanation is that SMT15 functions as both a positive and a negative cell-cycle regulator, with its relative contribution dependent on the status of the RB/E2F pathway and other pathways that are affected in the *smt* mutants. Having dual functions as a negative and a positive cell-cycle regulator is not unprecedented. For example, in mammalian cells the Cip/Kip proteins are general CDK inhibitors but also appear to play a positive role in the assembly or stabilization of cyclin D–CDK4 complexes (BOCKSTAELE *et al.* 2006).

***smt* mutants alter the commitment and mitotic checkpoint defects of *mat3*:** There are several ways that *smt*s might have suppressed the cell-size defects of *mat3-4*. One possible means of suppression was altered rates of

cell-cycle progression, leading to a slowed cell cycle and larger average cell size. We used dark-shift experiments to establish that the *smt*s suppressed *mat3-4* through alterations in cell-size checkpoint function. Although we have not accurately measured the time required for the *smt* mutants to transit the S/M phases of the cell cycle, our observations of partially synchronous cultures indicated that these mutants had no obvious defects in initiating and completing S phase, mitosis, and cytokinesis. These observations are also concordant with the absence of cell-cycle rate defects observed in *dp1* and *e2f1* mutant strains that also suppress *mat3-4* by altering size checkpoint regulation (Fang *et al.* 2006).

A second possibility for the *smt*s was that they might have suppressed only one of the two cell-size checkpoint defects evident in *mat3-4*, either the commitment defect or the daughter cell-size defect. However, as was the case for *dp1* and *e2f1* mutations, both of these size checkpoint defects in *mat3-4* were partially suppressed by each of the *smt*s (Table 6). These results strengthen the idea that the commitment and S/M size checkpoints are mechanistically coupled. Although as single mutants the *smt*s had very little overall effect on cell size, three of the four single *smt*s showed some defect at commitment, with *smt14-1* being the only mutant that showed no measurable difference compared with wild type. *smt7-1* and *smt16-1* strains both passed commitment at a larger size than wild type, and in the case of *smt7-1* this commitment phenotype was unstable, similar to what we previously observed for an *e2f1* suppressor mutation (Fang *et al.* 2006). In contrast to *smt7-1* and *smt16-1*, the *smt15-1* mutant passed commitment at a smaller size than wild type, but was still able to suppress the *mat3-4* commitment defect, indicating possible dual positive and negative roles in the cell cycle as discussed above. Overall, the phenotypes of the *smt*s reinforced the coupled nature of commitment and S/M size checkpoints and also highlighted the relative sensitivity of the commitment size checkpoint to perturbations. This differential sensitivity indicates that the size checkpoints at commitment and S/M are similar, but probably not identical, and that the S/M size checkpoint may be more robust or tightly regulated than the commitment size checkpoint.

Complex genetic interactions among *smt* mutants: The relatively weak suppression of *mat3-4* exhibited by the *smt*s led us to ask whether any stronger phenotypes could be revealed when *smt*s were combined with *dp1* mutations or with each other. Interestingly, none of the *smt*s showed synergism with the *dp1-1* null allele, suggesting that the SMT gene products act in conjunction with DP1/E2F1 to control the cell cycle, and not in separate or redundant pathways such as depicted in Figure 8A. While the genetic evidence we have obtained supports the idea that the SMTs function within the RB/E2F pathway, it does not completely rule out the relationship depicted in Figure 8A, where the SMTs converge on some common targets that are also regulated by E2F1/DP1. However, to accommodate our observations it would have to be argued that *dp1* mutants are completely blocked for the expression or activity of the common target loci such that there could be no further reduction caused by loss of SMT activity. Alternatively, the SMTs might regulate the activity or abundance of E2F1-DP1 as modeled in Figure 8B or act as downstream targets of E2F1-DP1, as modeled in Figure 8C. It should be noted that for the scenario depicted in Figure 8C, the SMTs need not be direct transcriptional targets of E2F1-DP1 or even transcriptionally regulated by the pathway. For example, in the case of *SMT7* we saw no increase in its message levels in a *mat3-4* background as would be predicted if it were a transcriptional target of the RB pathway.

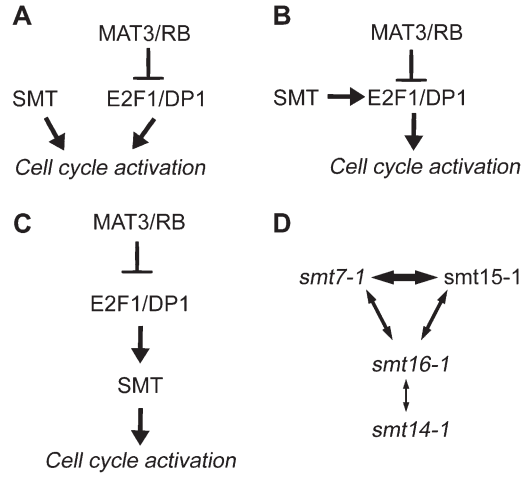

Figure 8.—Models for SMT function and genetic interactions. (A) SMT functioning separately from E2F1/DP1 to regulate the cell cycle. (B) SMT modulating the activity of E2F1/DP1. (C) SMT as a downstream effector of E2F1/DP1. (D) Schematic of genetic interactions between different *smt*s. Double arrows indicate a genetic interaction between indicated *smt*s with thicker lines indicating stronger interactions.

Although the *smt*s showed no genetic interactions with *dp1*, they showed complex interactions among themselves (Figure 8D). Most striking were the phenotypes of *smt7-1 smt15-1*, *smt7-1 smt16-1*, and *smt15-1 smt16-1* double mutants: Each of these combinations caused a large-cell phenotype in the absence of additional perturbation in the RB–E2F pathway (Table 7). Moreover, the large-cell phenotypes of these double mutants approached the severity of *dp1* null mutations, indicating that these *smt*s have defects in partially redundant cell-cycle activators that become limiting for size checkpoint function when they are simultaneously mutated. These results were important because they revealed that the *smt*s influenced the cell-cycle and cell-size checkpoint pathways of Chlamydomonas even when the canonical RB–E2F pathway was intact. Thus, the SMTs define *bona fide* cell-cycle regulators that must function properly for

MAT3/RB, E2F1, and DP1 to effectively control cell division in response to cell size.

A further layer of complexity was added to the synergistic interactions among *smt*s when MAT3 was removed. *smt7-1 smt15-1 mat3-4* triple mutants had severe size defects that were equivalent to those of the *smt7-1 smt15-1* double mutant or *dp1-1* single mutant. The insensitivity of *smt7-1 smt15-1* double mutants to loss of MAT3 suggests that E2F1/DP1 activity is effectively eliminated in the *smt7-1 smt15-1* double mutant. In contrast, the *smt7-1 smt16-1 mat3-4* and *smt15-1 smt16-1 mat3-4* triple mutants showed less severe cell size phenotypes compared to their *smt* double-mutant counterparts that contained wild-type MAT3 (Table 7). This latter result suggested that increased E2F1/DP1 activity (caused by loss of MAT3) could partially counteract the effect of *smt7-1 smt16-1* and *smt15-1 smt16-1* double-mutant combinations. Therefore, the canonical RB–E2F pathway was still at least partially functional in these latter two double-mutant strains.

Unlike the three cases discussed above, other combinations of *smt* alleles that involved *smt14-1* did not show strong genetic interactions. Only the combination of *smt14-1 smt16-1* showed weak additivity, causing a slightly large phenotype compared to wild type. A lack of genetic interaction between two mutants of similar phenotype could be interpreted to mean that the mutations affect the same pathway or complex. However, when the other genetic interactions between *smt*s are taken into consideration, this simple interpretation becomes difficult to envision since it would mean that SMT14 functions in the same pathway with at least two other SMTs, SMT7 and SMT15. On the other hand *smt7-1* and *smt15-1* showed strong interactions with each other, suggesting that they most likely function independently or redundantly with each other. Thus, there is no simple interpretation that accommodates all the genetic interaction data for the *smt*s as depicted in Figure 8D. Finally, the genetic interactions among the *smt*s can provide only clues about the nature of the RB–E2F pathway and cell-size checkpoint regulation. A further molecular analysis will be required to decipher their individual functions and how they interact with one another to control cell-size and cell-cycle progression.

***SMT7* encodes a putative SUMO-specific peptidase:** Post-translational modification by SUMO, small ubiquitin-like proteins, is a dynamic and reversible process in eukaryotes whose regulation requires different SUMO-specific peptidases. SUMO-specific peptidases have two major functions: They are required for processing SUMO precursors to their mature form, and they are also required to deconjugate SUMO from target proteins (Geiss-Friedlander and Melchior 2007). Sumoylation has been implicated in the control of multiple cell-cycle proteins (Muller *et al.* 2004; Ledl *et al.* 2005; Di Bacco and Gill 2006; Di Bacco *et al.* 2006), and failure to deconjugate SUMO can lead to defects in cell proliferation. For example, SUMO-specific peptidase Ulp1 is required for G_2/M progression in budding yeast (Li and Hochstrasser 1999). In mammalian cells, RNAi knockdown of SENP5—a human SUMO-specific peptidase—led to a dramatic decrease in cell proliferation (Di Bacco *et al.* 2006). In addition, several proteins that are important for cell-cycle control are regulated by sumoylation in a cell-cycle-dependent manner (Azuma *et al.* 2003; Joseph *et al.* 2004).

In Chlamydomonas, mutation in a potential SUMO-specific peptidase encoded by *SMT7* suppresses the small-cell-size phenotype of *mat3-4* and suggests that SMT7 functions a positive regulator of cell division. There are at least eight SUMO peptidases predicted from the version 3 draft of the Chlamydomonas genome (data not shown). Whether they act redundantly with SMT7 to regulate the cell cycle or function independently to control different cellular processes is yet to be determined. In addition, there are at least five potential SUMO or SUMO-like genes present in the Chlamydomonas genome (data not shown). It remains to be determined which ones are recognized by SMT7 and what are their target proteins. Functional characterization of SMT7 targets will help determine how sumoylation promotes RB/MAT3-regulated cell-cycle progression.

Chlamydomonas as a model organism for the RB pathway: Chlamydomonas is currently the only unicellular model in which the RB pathway can be probed genetically. The *smt* mutants that we identified define a set of cell-cycle regulators that function downstream of MAT3/RB to mediate size checkpoint control. The apparent complexity of their genetic interactions suggests that the *smt* mutations impinge on different aspects of the cell-cycle control machinery, which collectively regulate the decision to enter or exit the cell cycle. Chlamydomonas provides a useful alternative model for defining this network and for elucidating the mechanisms by which the RB pathway drives the cell cycle. Future studies will be aimed at cloning the remaining *SMT* genes and characterizing the mechanisms underlying SMT-mediated cell-cycle activation.

We thank Garrett Anderson for comments on the manuscript and for the pSI103 primers for adaptor-based isolation of flanking sequences. We thank Steve Pollock for the unpublished insertion-border isolation protocol. We thank Jimmie-Ray Austin, Tristan Harris, Clarence Pasion, Hiep Le, Jarrod Heck, and Jared Dennis for their technical assistance. This work was supported by the American Cancer Society (RSG-05-196-01-CCG to J.G.U.).

LITERATURE CITED

Andersen, E. C., X. Lu and H. R. Horvitz, 2006 C. elegans ISWI and NURF301 antagonize an Rb-like pathway in the determination of multiple cell fates. Development **133:** 2695–2704.

Armbrust, E. V., A. Ibrahim and U. W. Goodenough, 1995 A mating type-linked mutation that disrupts the uniparental inheritance of chloroplast DNA also disrupts cell-size control in Chlamydomonas. Mol. Biol. Cell **6:** 1807–1818.

Azuma, Y., A. Arnaoutov and M. Dasso, 2003 SUMO-2/3 regulates topoisomerase II in mitosis. J. Cell Biol. **163:** 477–487.

Bender, A. M., O. Wells and D. S. Fay, 2004 lin-35/Rb and xnp-1/ATR-X function redundantly to control somatic gonad development in C. elegans. Dev. Biol. **273:** 335–349.

Bender, A. M., N. V. Kirienko, S. K. Olson, J. D. Esko and D. S. Fay, 2007 lin-35/Rb and the CoREST ortholog spr-1 coordinately regulate vulval morphogenesis and gonad development in C. elegans. Dev. Biol. **302:** 448–462.

Berthold, P., R. Schmitt and W. Mages, 2002 An engineered Streptomyces hygroscopicus aph 7" gene mediates dominant resistance against hygromycin B in Chlamydomonas reinhardtii. Protist **153:** 401–412.

Bisova, K., D. M. Krylov and J. G. Umen, 2005 Genome-wide annotation and expression profiling of cell cycle regulatory genes in Chlamydomonas reinhardtii. Plant Physiol. **137:** 475–491.

Blais, A., and B. D. Dynlacht, 2004 Hitting their targets: an emerging picture of E2F and cell cycle control. Curr. Opin. Genet. Dev. **14:** 527–532.

Bockstaele, L., K. Coulonval, H. Kooken, S. Paternot and P. P. Roger, 2006 Regulation of CDK4. Cell Div. **1:** 25.

Bracken, A. P., M. Ciro, A. Cocito and K. Helin, 2004 E2F target genes: unraveling the biology. Trends Biochem. Sci. **29:** 409–417.

Cam, H., and B. D. Dynlacht, 2003 Emerging roles for E2F: beyond the G1/S transition and DNA replication. Cancer Cell **3:** 311–316.

Ceol, C. J., and H. R. Horvitz, 2001 dpl-1 DP and efl-1 E2F act with lin-35 Rb to antagonize Ras signaling in C. elegans vulval development. Mol. Cell **7:** 461–473.

Ceron, J., J. F. Rual, A. Chandra, D. Dupuy, M. Vidal *et al.*, 2007 Large-scale RNAi screens identify novel genes that interact with the C. elegans retinoblastoma pathway as well as splicing-related components with synMuv B activity. BMC Dev. Biol. **7:** 30.

Chaussepied, M., and D. Ginsberg, 2005 E2F and signal transduction pathways. Cell Cycle **4:** 392–396.

Craigie, R. A., and T. Cavalier-Smith, 1982 Cell volume and the control of the Chlamydomonas cell cycle. J. Cell Sci. **54:** 173–191.

Cui, M., D. S. Fay and M. Han, 2004 *lin-35/Rb* cooperates with the SWI/SNF complex to control *Caenorhabditis elegans* larval development. Genetics **167:** 1177–1185.

Cui, M., E. B. Kim and M. Han, 2006 Diverse chromatin remodeling genes antagonize the Rb-involved SynMuv pathways in C. elegans. PLoS Genet. **2:** e74.

Di Bacco, A., and G. Gill, 2006 SUMO-specific proteases and the cell cycle. An essential role for SENP5 in cell proliferation. Cell Cycle **5:** 2310–2313.

Di Bacco, A., J. Ouyang, H. Y. Lee, A. Catic, H. Ploegh *et al.*, 2006 The SUMO-specific protease SENP5 is required for cell division. Mol. Cell. Biol. **26:** 4489–4498.

Dimova, D. K., and N. J. Dyson, 2005 The E2F transcriptional network: old acquaintances with new faces. Oncogene **24:** 2810–2826.

Donnan, L., and P. C. John, 1983 Cell cycle control by timer and sizer in Chlamydomonas. Nature **304:** 630–633.

Ebel, C., L. Mariconti and W. Gruissem, 2004 Plant retinoblastoma homologues control nuclear proliferation in the female gametophyte. Nature **429:** 776–780.

Fang, S. C., C. de los Reyes and J. G. Umen, 2006 Cell size checkpoint control by the retinoblastoma tumor suppressor pathway. PLoS Genet. **2:** e167.

Fay, D. S., S. Keenan and M. Han, 2002 fzr-1 and lin-35/Rb function redundantly to control cell proliferation in C. elegans as revealed by a nonbiased synthetic screen. Genes Dev. **16:** 503–517.

Geiss-Friedlander, R., and F. Melchior, 2007 Concepts in sumoylation: a decade on. Nat. Rev. Mol. Cell. Biol. **8:** 947–956.

Harbour, J. W., and D. C. Dean, 2000 The Rb/E2F pathway: expanding roles and emerging paradigms. Genes Dev. **14:** 2393–2409.

Harris, E. H., 1989 *The Chlamydomonas Sourcebook—A Comprehensive Guide to Biology and Laboratory Use.* Academic Press, San Diego.

John, P. C., 1984 Control of the cell division cycle in Chlamydomonas. Microbiol. Sci. **1:** 96–101.

John, P. C. L., 1987 Control points in the Chlamydomonas cell cycle, pp. 9–16 in *Algal Development*, edited by W. Wiessner, D. G. Robinson and R. C. Starr. Springer-Verlag, Berlin.

Jordan, C. V., W. Shen, L. K. Hanley-Bowdoin and D. N. Robertson, 2007 Geminivirus-induced gene silencing of the tobacco retinoblastoma-related gene results in cell death and altered development. Plant Mol. Biol. **65:** 163–175.

Joseph, J., S. T. Liu, S. A. Jablonski, T. J. Yen and M. Dasso, 2004 The RanGAP1-RanBP2 complex is essential for microtubule-kinetochore interactions in vivo. Curr. Biol. **14:** 611–617.

Kindle, K. L., 1990 High-frequency nuclear transformation of Chlamydomonas reinhardtii. Proc. Natl. Acad. Sci. USA **87:** 1228–1232.

Knudsen, E. S., and K. E. Knudsen, 2006 Retinoblastoma tumor suppressor: where cancer meets the cell cycle. Exp. Biol. Med. **231:** 1271–1281.

Korenjak, M., and A. Brehm, 2006 The retinoblastoma tumour suppressor in model organisms–new insights from flies and worms. Curr. Mol. Med. **6:** 705–711.

Korenjak, M., B. Taylor-Harding, U. K. Binne, J. S. Satterlee, O. Stevaux *et al.*, 2004 Native E2F/RBF complexes contain Myb-interacting proteins and repress transcription of developmentally controlled E2F target genes. Cell **119:** 181–193.

Lavia, P., and P. Jansen-Durr, 1999 E2F target genes and cell-cycle checkpoint control. BioEssays **21:** 221–230.

Ledl, A., D. Schmidt and S. Muller, 2005 Viral oncoproteins E1A and E7 and cellular LxCxE proteins repress SUMO modification of the retinoblastoma tumor suppressor. Oncogene **24:** 3810–3818.

Lewis, P. W., E. L. Beall, T. C. Fleischer, D. Georlette, A. J. Link *et al.*, 2004 Identification of a Drosophila Myb-E2F2/RBF transcriptional repressor complex. Genes Dev. **18:** 2929–2940.

Li, S. J., and M. Hochstrasser, 1999 A new protease required for cell-cycle progression in yeast. Nature **398:** 246–251.

Litovchick, L., S. Sadasivam, L. Florens, X. Zhu, S. K. Swanson *et al.*, 2007 Evolutionarily conserved multisubunit RBL2/p130 and E2F4 protein complex represses human cell cycle-dependent genes in quiescence. Mol. Cell **26:** 539–551.

Lu, X., and H. R. Horvitz, 1998 lin-35 and lin-53, two genes that antagonize a C. elegans Ras pathway, encode proteins similar to Rb and its binding protein RbAp48. Cell **95:** 981–991.

Lumbreras, V., D. R. Stevens and S. Purton, 1998 Efficient foreign gene expression in Chlamydomonas reinhardtii mediated by an endogenous intron. Plant J. **14:** 441–447.

McAteer, M., L. Donnan and P. C. John, 1985 The timing of division in Chlamydomonas. New Phytol. **99:** 41–56.

Muller, S., A. Ledl and D. Schmidt, 2004 SUMO: a regulator of gene expression and genome integrity. Oncogene **23:** 1998–2008.

Ouellet, J., and R. Roy, 2007 The lin-35/Rb and RNAi pathways cooperate to regulate a key cell cycle transition in C. elegans. BMC Dev. Biol. **7:** 38.

Park, J. A., J. W. Ahn, Y. K. Kim, S. J. Kim, J. K. Kim *et al.*, 2005 Retinoblastoma protein regulates cell proliferation, differentiation, and endoreduplication in plants. Plant J. **42:** 153–163.

Ramirez-Parra, E., C. Frundt and C. Gutierrez, 2003 A genome-wide identification of E2F-regulated genes in Arabidopsis. Plant J. **33:** 801–811.

Reddien, P. W., E. C. Andersen, M. C. Huang and H. R. Horvitz, 2007 DPL-1 DP, LIN-35 Rb and EFL-1 E2F act with the MCD-1 zinc-finger protein to promote programmed cell death in *Caenorhabditis elegans*. Genetics **175:** 1719–1733.

Sizova, I., M. Fuhrmann and P. Hegemann, 2001 A Streptomyces rimosus aphVIII gene coding for a new type phosphotransferase provides stable antibiotic resistance to Chlamydomonas reinhardtii. Gene **277:** 221–229.

Staehling-Hampton, K., P. J. Ciampa, A. Brook and N. Dyson, 1999 A genetic screen for modifiers of E2F in *Drosophila melanogaster*. Genetics **153:** 275–287.

Stevaux, O., and N. J. Dyson, 2002 A revised picture of the E2F transcriptional network and RB function. Curr. Opin. Cell Biol. **14:** 684–691.

Umen, J. G., 2005 The elusive sizer. Curr. Opin. Cell Biol. **17:** 435–441.

Umen, J. G., and U. W. Goodenough, 2001 Control of cell division by a retinoblastoma protein homolog in Chlamydomonas. Genes Dev. **15:** 1652–1661.

Vandepoele, K., K. Vlieghe, K. Florquin, L. Hennig, G. T. Beemster *et al.*, 2005 Genome-wide identification of potential plant E2F target genes. Plant Physiol. **139:** 316–328.

Weinberg, R. A., 1995 The retinoblastoma protein and cell cycle control. Cell **81:** 323–330.

Wildwater, M., A. Campilho, J. M. Perez-Perez, R. Heidstra, I. Blilou *et al.*, 2005 The RETINOBLASTOMA-RELATED gene regulates stem cell maintenance in Arabidopsis roots. Cell **123:** 1337–1349.

Wyrzykowska, J., M. Schorderet, S. Pien, W. Gruissem and A. J. Fleming, 2006 Induction of differentiation in the shoot apical meristem by transient overexpression of a retinoblastoma-related protein. Plant Physiol. **141:** 1338–1348.

Zamora, I., J. L. Feldman and W. F. Marshall, 2004 PCR-based assay for mating type and diploidy in Chlamydomonas. Biotechniques **37:** 534–536.

Communicating editor: S. Dutcher